Experimental and kinetic modeling study of exo-TCD pyrolysis under low pressure

ARTICLE *in* COMBUSTION AND FLAME · MAY 2015

Impact Factor: 3.08 · DOI: 10.1016/j.combustflame.2015.01.015

5 AUTHORS, INCLUDING:

Guozhu Liu
Tianjin University
72 PUBLICATIONS **581** CITATIONS
SEE PROFILE

Li Wang
698 PUBLICATIONS **10,452** CITATIONS
SEE PROFILE

Combustion and Flame 162 (2015) 2177–2190

Contents lists available at ScienceDirect

Combustion and Flame

journal homepage: www.elsevier.com/locate/combustflame

Experimental and kinetic modeling study of exo-TCD pyrolysis under low pressure

Heng Li, Guozhu Liu *, Rongpei Jiang, Li Wang, Xiangwen Zhang

Key Laboratory for Green Chemical Technology of Ministry of Education, School of Chemical Engineering and Technology, Tianjin University, Collaborative Innovation Center of Chemical Science and Engineering, Tianjin 300072, PR China

ARTICLE INFO

Article history:
Received 4 December 2014
Received in revised form 20 January 2015
Accepted 21 January 2015
Available online 16 March 2015

Keywords:
Exo-TCD
Pyrolysis
Synchrotron vacuum ultraviolet photoionization mass spectrometry
Kinetic modeling

ABSTRACT

The exo-TCD (exo-tricyclo[5.2.1.$0^{2,6}$]decane) pyrolysis (3.0 vol.% exo-TCD in argon) was performed in a flow tube reactor at a temperature range of 900–1600 K under low pressure (667 Pa). The identification of products or intermediates and the isomeric distinction were accomplished by synchrotron vacuum ultraviolet photoionization mass spectrometry (SVUV-PIMS). Approximately 28 species were identified and quantified by near-threshold measurements of photoionization mass spectrum and photoionization efficiency spectrum. Meanwhile, the initial unimolecular decomposition rate of exo-TCD was estimated using transition states theory and Rice–Ramsperger–Kassel–Marcus (RRKM) theory. A detailed kinetic model of exo-TCD pyrolysis was developed including 316 species and 807 reactions. The simulation results generally agree well with the experimental data. ROP and sensitivity analysis indicate that under lower pressure the initial decomposition of exo-TCD is dominant by diradical channel rather than the unimolecular decomposition or H-abstraction channels, and that the methyl-cyclicC5 and methylene-cyclicC5 species may be one of the principal precursors for the formation of aromatics (benzene, toluene, etc.).

1. Introduction

Exo-TCD (exo-tricyclo[5.2.1.$0^{2,6}$]decane, see Fig. 1), is a kind of polycyclic hydrocarbon fuel for advanced aircrafts with the unique characteristics of high energy density, low freeze point, and high thermal stability [1–3]. It is also one of ideal candidates for the fuel-cooled thermal management system due to its significant endothermic capacity. In this case, the pyrolysis of this single component fuel would not only significantly enhance the endothermic heat sink but also produce significant amounts of olefins which are beneficial for the combustion in the fuel-cooled engine [4]. Consequently, it is crucial to elucidate detailed pyrolysis mechanism of exo-TCD for the design of thermal management system and corresponding combustors.

Previously, the comprehensive pyrolysis chemistry of exo-TCD has attracted lots of interests covering experiments, mechanism, and kinetics modeling, etc. [1,4–16]. As far as the experimental studies were concerned, much work had been performed to obtain the main products under various experimental conditions. An earlier shock tube experiment of exo-TCD ignition was performed by Davidson et al. [1,5] over the temperature range of 1200–1700 K under the pressure of 1–9 atm. They found that cyclopentene is the major initial decomposition product using the UV absorption spectrography to identify the products of exo-TCD decomposition. Nakra et al. [9] found that the main products from exo-TCD pyrolysis were ethylene, acetylene, propyne, C_4H_x, cyclopentadiene and benzene in micro-flowtube pyrolysis-mass spectrometry at the temperature up to about 1700 K with a residence time of the millisecond scale. Furthermore, the electron impact studies confirmed that the cyclopentadiene and benzene are the only significant C5 and C6 pyrolysis products. Rao and Kunzru [8] reported thermal cracking of exo-TCD in an annular tubular reactor at 903–968 K under atmospheric pressure, and found that the major products include methane, ethylene, propylene, cyclopentene, cyclopentadiene, benzene and toluene. Xing et al. [17] studied exo-TCD pyrolysis under the nearcritical and supercritical pressures, and observed the similar products at different experimental conditions. Park et al. [13] had performed a thermal decomposition experiment in a batch reactor and analyzed the primary decomposition products to explain the primary initiation mechanism of exo-TCD decomposition. They observed that 1-cyclopentylcyclopentene and 4-methyl-2,3,4,5,6,7-hexahydro-1H-indene are the main initial products directly from exo-TCD in the initial step of exo-TCD

* Corresponding author.
E-mail address: gliu@tju.edu.cn (G. Liu).

http://dx.doi.org/10.1016/j.combustflame.2015.01.015
0010-2180/

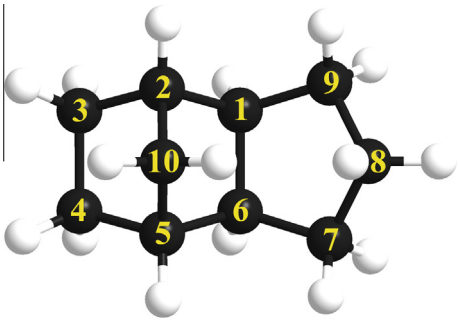

Fig. 1. The No. of C atoms for bond positions in exo-TCD molecular.

pyrolysis. Vandewiele et al. [14] measured the products of exo-TCD pyrolysis at the low and high conversion under 0.17 MPa, and discriminated cyclopentadiene as the primary product and benzene as the secondary products. Herbinet et al. [7] carried out a thermal decomposition experiment of exo-TCD (diluted with Helium) in a jet-stirred reactor from 848 to 933 K under atmospheric pressure and further built a detailed kinetic model using a diradical approach to describe the primary mechanism of the unimolecular initial step of tricyclodecane. The detailed kinetic model was generated by EXGAS program including one unimolecular initiation and six metathesis reactions with small radicals (hydrogen, methyl, and allyl radicals) for exo-TCD. The main decomposition mechanism could give satisfying predicted results for the reactant consumption and the yield of ethylene, cyclopentadiene, cyclopentene, toluene, 3-cyclopentylcyclopentene, while some small molecules are underestimated including hydrogen, methane, ethane and propene. This may be caused by the lacking of secondary reactions of intermediate-weight primary products with the possible carbon number range of C6–C10. Very recently, Magoon et al. [15,16] developed a highly detailed exo-TCD combustion model containing pyrolysis process applying the RMG software program and estimated intramolecular disproportionation reactions of diradicals based directly on ab initio calculations in the initial stage of exo-TCD pyrolysis. The results showed the pathway to 4-cyclopentylcyclopentene (CPCP-4) seems to be faster than the corresponding diradical pathway for temperatures less than 2000 K. Furthermore, Vandewiele et al. used this exo-TCD combustion model to simulate their experimental data and the agreement between experimental and modeling results suggested that RMG is a great potential program for building the detailed kinetic models of complex fuels pyrolysis [14]. Some major products of initial products of exo-TCD pyrolysis were shown in Scheme 1.

Furthermore, thermal decomposition experiment of exo-TCD was described by Bruno et al. [10] who also reported the measured or modeled thermochemical and thermophysical properties of exo-TCD for the further detailed mechanism and kinetic study. With the support of these data, Chenoweth et al. [11] performed molecular dynamics (MD) simulations at high temperatures and concluded that the thermal decomposition of exo-TCD initiated from C–C bond-scission mainly produced ethylene plus a C8 hydrocarbon or two C5 hydrocarbons including cyclopentene which also had been observed by Davidson et al. and Rao and Kunzru [1,8]. The consistency between the fitted rate constant from MD simulated data and the corresponding experimental values of Rao and Kunzru [1,8] verified the applicability of first-order kinetics for the overall thermal decomposition of exo-TCD at high temperature. From MD simulation, they also found that unstable C8 diradicals rapidly decompose to form 1,3-butadiene which is consistent with the products of Davidson et al. and Rao and Kunzru [1,8]. They observed the allyl radicals as the possible precursor of propene or propyne, while they did not observed benzene proposed by Davidson et al. [1,8] for its formation from secondary chemistry required much longer time than the simulation time. As the stable species, benzene was also observed by Rao and Kunzru [1,8] with the similar increased yield trend of methane and toluene. Though exo-TCD oxidation and pyrolysis over a wide range of experimental conditions were studied [4,7–9,13,14], little work has been done to identify the key radicals during the thermal cracking reaction, which will provide a new insight into the thermal decomposition chemistry of exo-TCD, especially the particular reaction channels.

In this study, we conduct an experiment of exo-TCD pyrolysis in a flowing tubular reactor under 667 Pa in a temperature range of 900–1600 K using SVUV-PIMS technique which is a reliable diagnostic method for radicals in pyrolysis, oxidation, combustion, etc. [18–23]. Meanwhile, the quantum chemical calculation was employed for the study of exo-TCD unimolecular decomposition mechanism and the corresponding reaction rate constants were further estimated by employing the Rice–Ramsperger–Kassel–Marcus (RRKM) theory. Based on the overall analysis of the reaction network linked the mechanisms of initial species, a detailed kinetic model was developed to simulate the exo-TCD pyrolysis. This work was mainly focused on the formation mechanism of benzene over the whole process of exo-TCD pyrolysis.

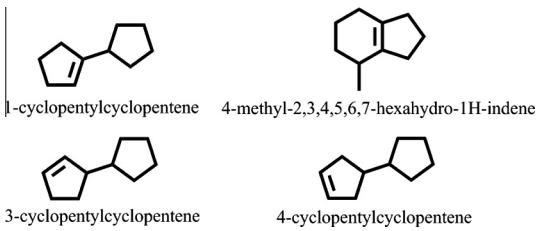

Scheme 1.

2. Experimental method

The exo-TCD fuel sample was self-synthetized by catalytic isomerization of endo-TCD (endo-tetrahydrodicyclopentadiene, made from hydrogenation of dicyclopentadiene [26]) using Al-grafted MCM-41 [24,25]. The purity of exo-TCD was about 99.1% measured by gas chromatograph.

The experimental work was conducted at National Synchrotron Radiation Laboratory (NSRL) in Hefei, China. The experimental equipments of SVUV-PIMS including two beamlines and the pyrolysis apparatus have been described in detail in some publications previously [18,20,23,27], which comprises of a pyrolysis chamber, a differentially pumped chamber, and a photoionization chamber with a homemade reflectron time-of-flight mass spectrometer (RTOF-MS), as seen in Fig. 2. The detailed experimental method has also been described in some previous Refs. [18,20,27]. In brief, the exo-TCD diluted with Ar was injected into a 6-mm-ID (inside diameter) and 300-mm-length alumina flow tube with 100 mm inside the furnace. Ar was controlled by a MKS mass flow controller with the flow rate of 970 SCCM (standard-state cubic centimeter per minute). Exo-TCD was feed by a syringe pump (ISCO 1000D) with the liquid flow rate of 0.1963 mL/min (approximately equivalent to 30 SCCM in gas phase) at room temperature. Besides, exo-TCD was vaporized and diluted with Ar in a vaporizer at the temperature of 360 K. Therefore, the total flow rate of the mixed gas was 1000 SCCM and the inlet mole fraction of exo-TCD equaled to 3.00%. Because there are so many more gas phase collisions than gas + surface collisions in the flow tube, we believe that wall catalysis can be neglected.

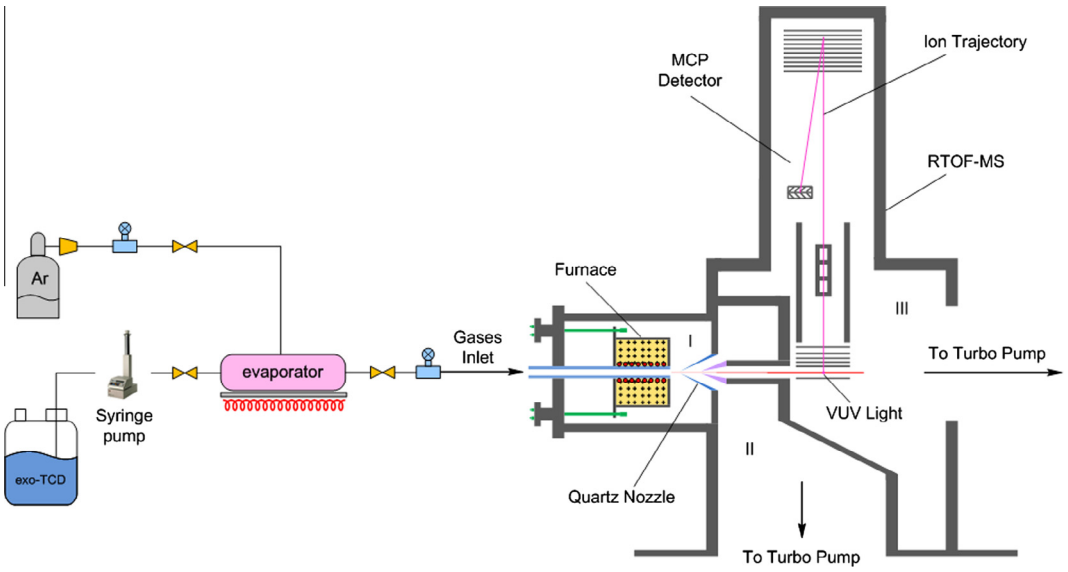

Fig. 2. Pyrolysis apparatus with molecular-beam sampling mass spectrometer.

The process of sampling has been described in detail in previous papers [28,29]. Briefly, the products sampling was performed by a quartz cone-like nozzle with a 40° cone angle at the tip in the process of the pyrolysis experiment. Subsequently, a molecular beam consisted of the sampled products was formed in the differentially pumped chamber and transported to the photoionization chamber by a nickel skimmer quickly, where it was irradiated by the tunable synchrotron vacuum ultraviolet VUV light. The ionized species generated were detected by RTOF-MS calibrated with a standard gas mixture (see Fig. S1).

The qualitative and quantitative analysis of pyrolysis species was achieved with two scanning modes of mass spectra in the experiment. The first mode was the measurement of photoionization efficiency (PIE) spectra with different photon energies at a fixed pyrolysis temperature, which could catch the ionization threshold of a special species and identify it through comparison with the ionization energy (IE) value from some authoritative literature. The PIE spectra of this experiment were taken at the pyrolysis temperature of 1480 K and the experimental error for determined IEs is within 0.05 eV due to the cooling effect of molecular beam [30]. The second one was the measurement of mass spectra with different pyrolysis temperatures at fixed photon energies, which could be used to evaluate the mole fraction of species accompanied with various temperatures. The calculation method of mole fraction has been described in detail previously [18,20]. More details on the gas expansion coefficients used in the mole fractions calculation was given in Fig. S2.

This experiment was kept at a low pressure of 667 Pa controlled by a MKS throttle valve. The temperature inside the tube was measured by the thermocouple (Pt 30% Rh/Pt 6% Rh) inserted into the heating region with the temperature uncertainty of ±2.5 K.

3. Theoretical calculation and kinetic model

3.1. Calculation method

The quantum chemical calculations are employed to analyze the initial unimolecular dissociation channels of exo-TCD by CBS-QB3 level, a complete basis set method combining CBS-Q energy calculations and the B3LYP/CBSB7 optimized geometries and frequencies [31,32]. The vibrational frequencies are computed at the B3LYP/CBSB7 level for characterizing the nature of structures and used for computing zero-point energy (ZPE) corrections. Several IEs of initial formed species are calculated applying the following formula:

$$\mathrm{IE}(M) = E(M^+) - E(M) \quad [33]$$

where M represents a kind of neutral molecular, M^+ is the cation of M, IE refers to the ionization energy, E indicates the electronic energy with ZPE. All the calculations were performed with the Gaussian09 program [34]. Relative energies and optimized geometries of the compounds and pertinent transition states are shown in the below.

3.2. Rate constant calculations

The rate constant calculation required parameters including reaction barriers, vibrational frequencies and rotational constants taken from the ab initio calculation. The rate constants of unimolecular decomposition channels with lower energy barriers were calculated by ChemRate program employing the RRKM/master equation method [35]. The molecular geometries and vibration frequencies of species involved in calculated unimolecular decomposition channels of exo-TCD are shown in Supplemental Material.

The interaction between reactant and the inert gas (Ar) is modeled by Lennard–Jones potential. Lennard–Jones parameters for exo-TCD and Ar were estimated by using following equations: [36]

$$\sigma = (2.3551 - 0.0874\omega)\left(\frac{T_c}{P_c}\right)^{1/3}$$

$$\varepsilon/k = (0.7915 + 0.1693\omega)T_c$$

where k is the Boltzmann constant. The critical temperature (T_c) and critical pressure (P_c) of exo-TCD was taken from the research of Bruno et al. [10] and the corresponding acentric factor (ω) is estimated by the Pitzer method [37]. Furthermore, the critical properties for Ar were taken from the NIST database.

The energy transfer per download collision was calculated by a single-parameter exponential down model in Ar, which can be described as $\langle \Delta E_{down} \rangle = 2000\ \mathrm{cm}^{-1}$. da Silva et al. [38] had found that a $\langle \Delta E_{down} \rangle$ value on the order of 2000 cm^{-1} could accurately reproduce the experimental falloff behavior at higher

temperatures in the calculation of rate constant for thermal decomposition of the benzyl radical.

3.3. Kinetic model construction

The chemical kinetic model was developed consisting of 316 species and 807 reactions involving the primary reaction mechanisms and the corresponding submechanism. Table 1 and Table S1 list some key reactions and species with formulas in this kinetic model of exo-TCD pyrolysis respectively.

The initial reactions contain the diradical mechanisms and unimolecular decomposition mechanisms of exo-TCD. The diradical mechanisms are taken from the pyrolysis model of Herbinet et al. [7,39]. The reverse reaction rate constants of the channels (exo-TCD = BR1 and exo-TCD = BR2) are deduced from the Refs. [7,39,40]. Some unimolecular decomposition mechanisms with rate constants are calculated in this work. The sub-mechanisms covered the species from the initial products to the C5–C10 species are mainly derived from some reaction models of exo-TCD and toluene in some previous published Refs. [7,15,41] and some mechanisms generated by RMG program [42]. Furthermore, some sub-mechanisms below C6 are taken from cyclohexane pyrolysis model [43], which contained the C0–C2 mechanisms derived from the GRI 3.0 mechanism [44] and some principal mechanisms supported by JetSulf 2.0 [45]. Most of thermodynamic and transport properties are available in each model while the missing parameters are generated by RMG program [42]. The kinetic simulation was performed through the ChemkinPRO program [46]. The complete mechanism for exo-TCD pyrolysis is presented in Supplementary Material.

This model was developed to predict the products distribution of exo-TCD pyrolysis. Therefore, the mechanism should be verified at wide range of pressure and temperature conditions and against to measurements and data published already. While most of the model parameters were computed or from literature and were not adjusted, we adjusted the values of 8 rate coefficients to better fit this experimental data. This model is just a tentative version with lots of rates estimated. The details are given in the Supplementary Material.

4. Results and discussion

4.1. Identification of pyrolysis species

Species formed in exo-TCD pyrolysis were identified using SVUV-PIMS. The pure exo-TCD photoionization spectrum was measured and shown in Fig. 3. The obvious onset gives the IE 9.32 eV agreeing well with the value 9.35 ± 0.05 eV from NIST database (http://webbook.nist.gov/chemistry/).

The lumped photoionization mass spectra at 1320 K were measured at seven different photon energies ranging from 8.5 to 11.7 eV (Fig. S3). The seven photon energies from 8.5 to 11.7 eV are applied for the measurement of photoionization mass spectra to ensure all species with their IEs covered wide IE range can be exactly detected at the near-threshold photoionization condition and reduce the impact of fragments. A number of peaks with m/z = 15–136 revealed on the mass spectrum covering the C1–C10 hydrocarbons.

Therefore, most species can be identified by the above mode but some isomers were differentiated by high-resolution PIE spectra (see Fig. S4). The PIE spectrum is generated by the integrated ion signals of each mass peak normalized by photon flux plotted versus the photon energy providing the precise information of the ionization thresholds [47], which were used to identify species by comparing ionization energies (IEs) with the literature. For instance, there is an obvious onset at 9.22 eV on the PIE spectra of m/z = 136 (see Fig. S4(a), corresponding to the ionization of exo-TCD (IE = 9.35 eV [48]). Moreover, the reactant may even be accompanied with some isomers, especially in the initial decomposition stage [13]. The visible onset at 8.82 eV is found on the same ionization curve relating to the isomers of exo-TCD photoionization and deduced to be the 4-methyl-2,3,3a,4,5,7a-hexahydro-1H-indene (ID6H4M67e), 4-cyclopentylcyclopentene (CPCP-4) or 3-cyclopentylcyclopentene (CPCP-3). Unfortunately, they cannot be distinguished because their IEs are so similar (ID6H4M67e: 8.75, CPCP-4: 8.87 and CPCP-3: 8.82 eV calculated at CBS-QB3 level). However, the species corresponding to the onset at 8.82 eV may be a trace of initial products of exo-TCD pyrolysis. Besides, these isomers have been investigated by Magoon during the study of the intramolecular disproportionation and ring-opening of exo-TCD [15]. Further, an onset can be observed at 10.64 eV, which may be caused by some ion fragments.

Analogously, there are two onsets at 9.65 and 10.37 eV in the PIE spectra of m/z = 40, corresponding to the ionization of allene (IE = 9.69 [49]) and propyne (IE = 10.36 [50]) respectively. Besides, the onsets at 8.38 and 9.25 eV on the PIE spectrum of m/z = 78 (see Fig. S4(c)) related to the ionization of fulvene (IE = 8.36 eV [51]) and benzene (IE = 9.24 eV [50]). Another PIE spectrum of m/z = 92 (see Fig. S4(d)) with the onsets at 7.90 and 8.85 eV, are attributed to the ionization of 5-methylene-1,3-cyclohexadiene (IE = 7.90 eV [52]) and toluene (IE = 8.828 eV [53]) respectively. The PIE spectra of m/z = 65 and m/z = 66 are related to the species of cyclopentadienyl (IE = 8.41 eV [54]) and cyclopentadiene (IE = 8.57 eV [55]), which are reflected by the two onsets locating at 8.48 eV and 8.59 eV (see Fig. S4(e)). The two species are the primary products during the exo-TCD pyrolysis.

4.2. The mole fraction profiles

The near-threshold photoionization mass spectra measured at different temperatures can be applied to evaluate the mole fraction of observed pyrolysis species. The photoionization mass spectra (as shown in Fig. S5) are measured with the photon energy of 11.7 eV at 970, 1170, 1270, 1350, 1420 and 1470 K respectively. Their initial formation temperature (T_{form}), the maximum mole fraction (X_M) and the corresponding temperatures (T_M) of the identified species are listed in Table 2 with their experimental IEs and those from literatures. It should be noted that only species with mole fraction larger than 10^{-5} were indentified and listed.

Figures 4 and 5 show the mole fraction values of exo-TCD (exo-tetrahydrodicyclopentadiene), and some important products and intermediates, for example, hydrogen (H_2), methyl (CH_3), methane (CH_4) and ethylene (C_2H_4). The initial decomposition temperature of exo-TCD is about 970 K. It gradually declines until almost complete decomposition at 1600 K. Simultaneously, accompanied with exo-TCD decomposition, the C0–C2 species including hydrogen, methyl, methane and ethylene increase continuously until the temperatures corresponding to their maximum mole fraction values (T_M) all at 1600 K. The formation temperatures (T_{form}) of H_2, CH_4 and C_2H_4 are all at 1090 K respectively. The T_{form} of CH_3 is at 1200 K. The mole fraction values of C3 species including allene (aC_3H_4), propyne (pC_3H_4), allyl (aC_3H_5), propylene (C_3H_6) and propargyl (C_3H_3) are shown in Fig. 5(e)–(i). The T_{form} of aC_3H_4, pC_3H_4 and aC_3H_5 are all at 1200 K while the T_{form} of C_3H_6 and C_3H_3 are at about 1100 and 1300 K respectively. After the initial formation, aC_3H_4, pC_3H_4 and C_3H_3 grow as the increasing temperature until their T_M at 1600 K while aC_3H_5 and C_3H_6 both have a convex parabolic tendency and their T_M are at 1450 and 1550 K respectively. Figure 5(j)–(m) shows the mole fraction values of C4–C5 species including 1-butene(C_4H_8-1),

Table 1
The rate constants of some key reactions in this model for exo-TCD pyrolysis, $k = AT^n exp(-E/RT)$. The units are in cm^3, mol, s, cal.

Selected reactions		A	n	E	Ref.
Reactions of exo-TCD					
1	exo-TCD = BR1	1.30E+15	0	77,000	[7], [a]
	REV/	1.12E+10	0	4270 /	[7,39]
2	exo-TCD = BR2	1.26E+15	0	71,000	[7], [b]
	REV/	6.70E+18	0	24,000 /	[7,39,40]
3	BR1 = CPCP-3	1.88E+10	1	7750	[7]
4	BR2 = ID7H4YM	9.70E+09	0.984	17,500	[7] [39]
5	exo-TCD = CPCP-4	1.73E+27	−3.52647	91374.6	This work[c]
6	exo-TCD = CPCP-3	1.05E+38	−6.76017	114,805	This work[c]
7	exo-TCD = NBeP1	3.04E+32	−5.2103	90317.4	This work[c]
8	exo-TCD = NBM2Ee1	5.51E+34	−5.75005	102,308	This work[c]
9	exo-TCD = NBAl1	4.79E+33	−5.47794	93276.8	This work[c]
10	exo-TCD = ID6H4M67e	2.36E+29	−4.37665	93182.3	This work[c]
11	exo-TCD + H = exo-TCDJ4 + H2	4.47E+06	2	5000	[7]
12	exo-TCD + H = exo-TCDJ1 + H2	4.47E+06	2	5000	[7]
13	exo-TCD + H = exo-TCDJ3 + H2	4.17E+06	2	2400	[7]
14	exo-TCD + H = exo-TCDJ2 + H2	4.17E+06	2	2400	[7]
15	exo-TCD + H = exo-TCDJ5 + H2	4.47E+06	2	5000	[7]
16	exo-TCD + H = exo-TCDJ6 + H2	4.47E+06	2	5000	[7]
17	exo-TCD + CH3 = exo-TCDJ4 + CH4	5.80E+06	1.77	8530	[15]
18	exo-TCD + CH3 = exo-TCDJ1 + CH4	5.80E+06	1.77	8530	[15]
19	exo-TCD + CH3 = exo-TCDJ3 + CH4	1.15E+06	1.83	6940	[15]
20	exo-TCD + CH3 = exo-TCDJ2 + CH4	1.15E+06	1.83	6940	[d]
21	exo-TCD + CH3 = exo-TCDJ5 + CH4	5.80E+06	1.77	8530	[e]
22	exo-TCD + CH3 = exo-TCDJ6 + CH4	5.80E+06	1.77	8530	[e]
Reactions of C10H16 products					
23	CPCP-3 = BR60	5.00E+15	0	65,200	[7]
24	BR60 = cC5H9 + C5H7Y2	3.30E+13	0	22,500	[7]
25	cC5H9 + cC5H7J3 = CPCP-4	3.25E+14	−0.7	0	[f]
26	C2H4 + CP2e2P = NBeP1	1.71E+10	0	23361.82	[g]
27	C2H5 + CPeJ4YM3 = CP2e2P	1.00E+13	0	0	[f]
28	CPeJ4YM3 = CPe3CH24J3	5.77E+12	0.02	1585	[f]
29	CPe4CH25J3 = CPe3CH24J3	6.96E+13	1.95	19,260	[f]
30	SAXcC6H7 = CPe4CH25J3	1.00E+10	0	25,850	[f]
31	aC3H5 + NBAJ = NBAl1	4.79E+08	−0.75	0	[f]
32	cC6eYM4 = NBAJ	2.51E+10	0	6850	[f]
33	aC3H5 + C4H6 = cC6eYM4	6.83E+10	0	23361.82	[f]
34	ID6H4M78eJJ = ID6H4M67e	1.13E+11	1.00E+00	3850	[15]
35	ID6H4M78eJJ = ID6H4M38e	5.66E+10	1.00E+00	3850	[15]
36	cC5H6YM1YE2 + C2H4 = ID6H4M38e	1.71E+10	0	23361.82	[15]
37	cC5H5E1YM2 = cC5H6YM1YE2	1.13E+11	1	7750	[15]
38	cC5H5M1YE2 = cC5H6YM1YE2	1.70E+11	1	7750	[15]
39	cC5H5E1YM2 = cC5H5YM3E2	1.13E+11	1	7750	[15]
40	CPeJ2YM3 + C2H5 = cC5H5YM3E2	4.79E+14	−0.75	0	[15]
41	fulvene + H = CPeJ2YM3	5.70E+13	0	4300	[15]
42	cC5H5M1YE2 = cC5H6E1M2	2.26E+11	1	7750	[15]
43	CH3 + cC5H4YM3M2 J = cC5H6E1M2	3.30E+12	0	0	[f]
44	cC5H6M1YM5 + H = cC5H4YM3M2 J	2.85E+13	0	4300	[f]
45	cC5H6M1YM5JJ = cC5H6M1YM5	2.51E+09	0	0	[f]
46	cC5H6M1YM5JJ = CPeJ23M4YM5	1.13E+11	1	16,300	[f]
47	CP2eYM15 = CPeJ23M4YM5	1.13E+11	1	7750	[f]
48	CP2eYM15 = CPe4CH25YM3	1.16E+13	0.02	1585	[f]
49	CHeYM4J35 = CPe4CH25YM3	5.77E+12	0.02	1585	[f]
50	CHeYM4J35 = A1CH3	2.26E+11	1	7750	[f]
51	A1CH2 + H(+M) = A1CH3(+M)	7.22E+13	0.062	−44	[58]
Reactions of C10H15 radicals					
52	CPJ2CPe4 = exo-TCDJ1	5.02E+10	0	6850	[15]
53	cC5H7J3 + cC5H8 = CPJ2CPe4	3.47E+11	0	12133.33	[15]
54	cC5H7cC5H8J3 = exo-TCDJ4	2.51E+10	0	6850	[15]
55	BCPe34 + H = cC5H7cC5H8J3	2.00E+13	0	2900	[15]
56	cC5H8J13 + C5H7 = cC5H7cC5H8J3	6.50E+14	−0.7	0	[15]
57	cC5H7J3 + C5H7 = BCPe34	4.88E+14	−0.7	0	[15]
58	Pl6H4EJ = exo-TCDJ3	2.51E+10	0	6850	[f]
59	C2H4 + Pl6HJ4 = Pl6H4EJ	3.46E+11	0	7000	[f]
60	CP2e2PJ = Pl6HJ4	2.51E+10	0	6850	[f]
61	C2H4 + CPeJ4YM3 = CP2e2PJ	1.43E+12	0	14,400	[f]
62	NB12eYP = exo-TCDJ2	2.51E+10	0	10749.37	[f]
63	CPJ-3YC5J14 = NB12eYP	5.07E+11	0.07	1960	[f]
64	CPJ-3YC5J14 = CPe4YC5 J	2.26E+11	1	3850	[f]
65	C2H4 + CPe4YPJ = CPe4YC5 J	3.98E+03	2.44	5370	[f]
66	CPe4YPJ = CPe4YPJ3	2.12E+06	1.58	12,070	[f]
67	CH3 + CP2eV1 = CPe4YPJ3	7.30E+12	0	5700	[f]
68	NBJ2Al1 = exo-TCDJ5	3.58E+07	1.12	25365.8	[f]

(*continued on next page*)

Table 1 (*continued*)

Selected reactions		*A*	*n*	*E*	Ref.
69	aC3H5 + NBe = NBJ2Al1	2.48E+10	0.24	10487.5	[f]
70	C2H4 + C5H6 = NBe	1.71E+10	0	23361.82	[g]
71	CPJ2CPe3 = exo-TCDJ6	1.36E+10	0	26516.67	[f]
72	cC5H8 + C5H7 = CPJ2CPe3	3.47E+11	0	12133.33	[f]
Reactions of C6 species					
73	A1- + H2 = A1 + H	5.71E+04	2.43	6273	[45]
74	A1- + H = A1	8.02E+19	−2	1968	[43]
75	A1- + CH4 = A1 + CH3	3.89E−03	4.6	5256	[59]
76	A1 + C2H3 = A1C2H3 + H	3.59E+12	0	6400	[43]
77	A1CH3 + H = A1 + CH3	1.93E+06	2.17	4163	[59]
78	C4H4 + C2H2 = A1	4.47E+11	0	30,010	[60]
79	A1 + C3H3 = C9H8 + H	6.26E+09	2.61	56,500	[41]
80	C3H3 + C3H3 = A1	1.64E+66	−15.9	27,529	[61]
81	C3H3 + C3H3 = A1	1.20E+35	−7.4	5058	[61]
82	C3H3 + C3H3 = A1- + H	2.02E+33	−6	15,940	[61]
83	SAXcC6H7 = A1 + H	2.64E+59	−14.35	44,929	[62]
84	fulvene + H = A1 + H	3.00E+12	0.5	2000	[61]
85	fulvene = A1	5.62E+81	−19.4	121,500	[61]
86	C3H3 + C3H3 = fulvene	7.25E+65	−16	25,035	[61]
Reactions of C5 species					
87	C5H7Y2 = C5H7	1.05E+07	1.19	34911.6	[f]
88	lC5H7 = C5H7Y2	3.20E+14	0	35961.8	[63]
89	aC3H5 + C2H2 = lC5H7	1.00E+12	0	6881.7	[63]
90	H + C5H7 = H2 + C5H6	3.62E+12	0	0	[15]
91	cC5H8 = C5H6 + H2	1.00E+12	0	61,000	[64]
92	C5H6 + H = C5H5 + H2	3.00E+14	0	6600	[15]
93	C5H6 = C2H2 + aC3H4	3.80E+17	0	104,000	[15]
94	C5H5 + H = C5H6	1.00E+14	0	0	[15]
95	C5H6 + CH3 = C5H5 + CH4	5.00E+11	0	5000	[65]
96	C5H6 + H = C2H2 + aC3H5	7.74E+36	−6.18	32,890	[59]
97	C5H5 = lC5H5	1.64E+96	−23.5	137,409	[43]
98	C5H5 + H = cC5H4 + H2	3.23E+07	2.095	15,842	[43]
99	A1CH2 = C5H5 + C2H2	3.00E+12	0	70,000	[43]
100	C2H3 + C3H3 = lC5H5 + H	1.00E+13	0	0	[59]
101	lC5H5 + CH3 = C5H4 + CH4	1.95E+13	−0.5	0	[43]
102	lC5H5 + H = C5H4 + H2	1.81E+12	0	0	[43]
103	cC5H7J3 = C5H7	1.31E+11	0.638	39,880	[15]
104	cC5H7J3 = C5H7	8.19E+08	1.13807	34789.75	[15]
105	C5H7 + H = cC5H8J13	1.22E+13	0	3300	[15]
106	H + cC5H8 = H2 + C5H7	4.47E+08	2.36	1110	[h]
107	cC5H9(+M) = PXC5H9(+M)	6.03E+12	0.07	27982.9	[43]
108	Pe2J15 = cC5H8	1.55E+10	0.31	1700	[f]
109	Pe2J15 = C5H8–13	1.13E+11	1	7750	[f]
110	PXC5H9 = C5H8–13 + H	1.27E+24	−4.75	23,777	[43]
111	PXC5H9 = cC5H9	1.22E+08	1.05	15,820	[15]
112	C5H6 + H = C5H7	2.00E+13	0	0	[f]
113	aC3H5 + C2H3 = lC5H7 + H	1.00E+13	0	0	[59]
114	C5H6 + C2H3 = C5H5 + C2H4	6.00E + 12	0	0	[65]
115	C4H5-2 + C2H4 = C5H6 + CH3	5.00E + 14	0	25,000	[59]
116	C5H10(+M) = aC3H5 + C2H5(+M)	2.20E+15	0	70,000	[43]
Reactions of C0–C4species					
117	C4H81 + H = C3H6 + CH3	3.20E+22	−2.39	11,180	[43]
118	C4H81 + H = C2H4 + C2H5	8.80E+16	−1.05	6461	[43]
119	aC3H5 + CH3(+M) = C4H81(+M)	1.00E+14	−0.32	−262	[59]
120	pC4H9 = C4H81 + H	8.00E+27	−5.613	29,791	[43]
121	aC3H5 + aC3H5 = pC3H4 + C3H6	8.43E+10	0	−263	[66]
122	aC3H5 + H(+M) = C3H6(+M)	2.00E+14	0	0	[45]
123	aC3H4 + H = aC3H5	4.80E+61	−14.67	26,000	[43]
124	pC3H4 + H = aC3H5	5.50E+59	−14.56	28,100	[43]
125	pC3H4 = aC3H4	3.20E+61	−14.59	88,200	[43]
126	aC3H4 + H = C3H3 + H2	6.60E+03	3.1	5522	[43]
127	aC3H4 + CH3 = C3H3 + CH4	6.60E−04	5	8300	[66]
128	aC3H5 + CH3 = aC3H4 + CH4	3.01E+12	−0.32	−130	[66]
129	aC3H5 + H = aC3H4 + H2	3.45E+06	2.07	4955	[66]
130	pC3H4 + H = C3H3 + H2	3.57E+04	2.8	4821	[43]
131	pC3H4 = C3H3 + H	3.70E+44	−9.06	100,390	[43]
132	H + pC3H4 = C2H2 + CH3	3.89E+10	0.989	4114	[43]
133	C3H3 + aC3H5 = fulvene + 2H	3.26E+29	−5.4	3390	[61]
134	C6H10-15 = aC3H5 + aC3H5	1.07E+80	−19.33	95,177	[43]
135	C2H3 + CH3 = aC3H5 + H	1.50E+24	−2.83	18,618	[45]
136	H + aC3H4 = H + pC3H4	1.47E+13	0.26	4103	[43]
137	C3H3 + H = C3H2 + H2	1.00E+13	0	1000	[59]
138	C2H4 + aC3H5 = PXC5H9	1.43E+12	0	14,400	[15]
139	C2H2 + CH2 = C3H3 + H	1.20E+13	0	6620	[59]

Table 1 (*continued*)

Selected reactions		*A*	*n*	*E*	Ref.
140	PAXCH2-2-1C4H7 = aC3H4 + C2H5	2.32E+24	−4.8	25,054	[43]
141	H + aC3H4 = CH3 + C2H2	2.72E+09	1.2	6834	[43]
142	H + C2H4(+M) = C2H5(+M)	5.40E+11	0.45	1820	[44]
143	CH3 + CH3 = H + C2H5	4.99E+12	0.1	10,600	[44]
Reactions of C9 species					
144	C9H8 + H = C9H7 + H2	2.80E+13	0	2258.6	[67]
145	C9H7 + H(+M) = C9H8(+M)	1.00E+14	0	0	[i]
146	C9H8 + CH3 = C9H7 + CH4	1.80E−01	4	456.5	[67]
147	A1- + aC3H4 = C9H8 + H	5.13E+02	3.2	2788	[43]
148	A1CH ∗ CHCH2 = C9H8 + H	1.40E+11	0	16,200	[j]
149	A1- + C3H3 = C9H8	1.50E+75	−17.8	39,600	[43]
150	A1CH2 + C2H2 = C9H8 + H	3.16E+04	2.5	11061.2	[67]

[a] Reduced by a factor of 5 considering the effect of low pressure.
[b] Reduced by a factor of 5 considering the effect of low pressure.
[c] The adjusted factor seen in Supplementary Material.
[d] Rate constant estimated by analogy with the values of exo-TCD + CH_3 = exo-TCDJ3 + CH_4 [15].
[e] Rate constant estimated by analogy with the values of exo-TCD + CH_3 = exo-TCDJ1 + CH_4 [15].
[f] Generated by RMG program [42].
[g] Rate constant estimated by analogy with the values of cC5H6YM1YE2 + C_2H_4 = ID6H4M38e [15].
[h] Rate constant estimated by analogy with the values of H + cC_5H_8 = H_2 + C_5H_7 [15].
[i] Rate constant estimated by analogy with the values of C_5H_5 + H (+M) = C_5H_6 (+M) [59].
[j] Rate constant estimated by analogy with the values of A1CH * CHCH2 = C_9H_8 + H [68].

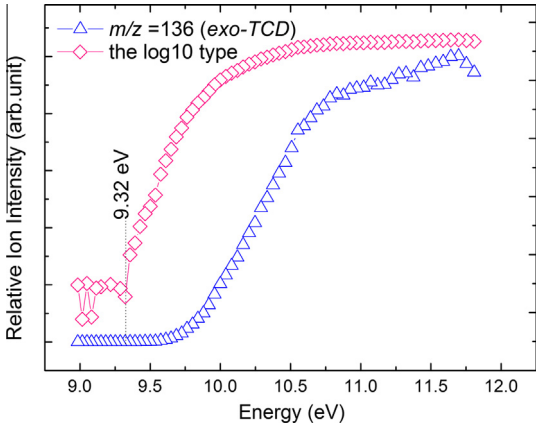

Fig. 3. PIE spectrum of pure exo-TCD.

cyclopentadienyl(C_5H_5), cyclopentadiene(C_5H_6) and 1,3-penta diene(C_5H_8-13). C_4H_8-1 starts to grow at 1100 K and reach a maximum value at 1470 K and then decrease gradually. The C5 species including C_5H_5, C_5H_6 and C_5H_8-13 start to form at 1200 K and grow as the increasing temperature until their T_M at 1600 K. The mole fraction values of fulvene, benzene (A1), benzyl ($A1CH_2$), phenylacetylene ($A1C_2H$) and indene (C_9H_8) are shown in Fig. 5(n)–(r). The T_{form} of fulvene, $A1CH_2$ and $A1C_2H$ are all at 1200 K while the T_{form} of A1 and C_9H_8 are at 1100 and 1370 K respectively. As the increasing temperature, these species all exhibit a monotonically increasing trend until 1600 K.

4.3. Theoretical calculation

The initial unimolecular decomposition of exo-TCD starts with the splitting of C–C bonds or C–H bonds. As shown in Table S2, the C–H bond dissociation energies (BDEs) for exo-TCD calculated at CBSQB3 level are 97.5 (C3/C4-H, exo-TCDJ1-H), 106.1 (C2/C5-H, exo-TCDJ2-H), 98.9 (C1/C6-H, exo-TCDJ3-H), 94.9 (C9/C7-H, exo-TCDJ4-H), 95.2 (C8-H, exo-TCDJ5-H) and 101.5 (C10-H, exo-TCDJ6-H) kcal mol^{-1}, which are consistent with the literature values [56] at the same site. While, the C–C BDEs calculated at CBSQB3 level by Bozzelli et al. [57] are at the range of 69–80 kcal mol^{-1}, which are much lower than C–H BDEs. Therefore, the C–C bond dissociation type reaction is the lowest energy pathway of all the unimolecular decomposition pathways.

The intramolecular C–C bonds fission may take place in seven locations in the initial reaction step as reported by Herbinet et al. [7]. The C–C BDEs of reactant molecular are different associated with the various locations, which has also been studied by Bozzelli et al. [57]. Their calculation results of BDEs indicate that the BDE (C2–C10) and (C1–C2) have the lower energies which is also supported by the theory of their lower diradical ring strain energy and higher lost ring strain energy. Jiao et al. [12] had studied the electron impact ionization of exo-TCD using Fourier transform mass spectrometry and analyzed the bond strain energy of exo-TCD molecular, which suggested the bond (Bridge bond) between C10 and C2 or C5 atom is the possible cleavage site and the corresponding energy barrier is lower than other bond cleavages channels. Park et al. [13] also reported CPCP-1 and 4-methyl-2,3,4,5,6,7-hexahydro-1 H-indene were the primary species at the initial step of exo-TCD thermal decomposition, which also suggested that the primary products are from the C1–C2 and C2–C10 bond scission respectively. Although the initial products between the previous studies of various researchers are different, it could not deny that the existence of cyclopentylcyclopentene and methylindene. The resemblance of molecular structural characteristics of initial products suggests the probable similarity of forming pathways for the key species from exo-TCD initial pyrolysis. Therefore, the first scission site may probably be started from the C1–C2 or C2–C10 bond scission.

Some calculated possible unimolecular decomposition pathways of exo-TCD pyrolysis involved the reactants, transition states, intermediates and products are displayed in Fig. S6. The optimized molecular geometries are listed in Fig. S7. Most primary decomposition channels of exo-TCD usually produce the intermediates with double bonds through the H-transfer process of diradicals. The pink mark represents the channels with lower energy barrier including TS1, TS8, TS18, TS10 and TS12. 4-cyclopentylcyclopentene (CPCP-4: PC1) and 4-methyl-2,3,3a,4,5,7a-hexahydro-1H-indene (ID6H4M67e: PC8) are formed by the open-ring reactions from the bonds scission at C1–C2 and C2–C10 sites of exo-TCD molecular via the transition states TS1 and TS8 surmounting the lower energy barriers of 82.44 and 83.82 kcal mol^{-1}, which is consistent with some previous studies about the initial bond scission

Table 2
List of the produced species measured in the exo-TCD pyrolysis.

m/z	Formular	Species	IE (eV)		X_M[c]	T_{form} (K)[d]	T_M (K)[e]
			Literature[a]	This work[b]			
2	H_2	Hydrogen	15.43	15.43	3.01E−02	1090	1600
15	CH_3	Methyl	9.84	9.83	3.76E−03	1200	1600
16	CH_4	Methane	12.61	12.60	3.85E−03	1090	1600
26	C_2H_2	Acetylene	11.40	11.40	8.59E−03	1090	1600
28	C_2H_4	Ethylene	10.51	10.52	3.27E−02	1090	1600
29	C_2H_5	Ethyl	8.11	8.63	4.55E−05	1200	1450
39	C_3H_3	Propargyl	8.67	8.73	3.24E−03	1300	1600
40	C_3H_4	Allene	9.69	9.65	3.06E−03	1200	1600
	C_3H_4	Propyne	10.36	10.37	3.36E−03	1200	1600
41	C_3H_5	Allyl	8.18	8.19	5.56E−03	1200	1450
42	C_3H_6	Propene	9.73	9.72	4.32E−03	1090	1550
52	C_4H_4	Vinylacetylene	9.58	9.58	1.48E−03	1350	1600
54	C_4H_6	1,3-Butadiene	9.07	9.08	2.97E−03	1200	1600
56	C_4H_8	1-Butene	9.55	9.61	2.06E−03	1090	1470
65	C_5H_5	Cyclopentadienyl	8.41	8.48	6.16E−03	1200	1600
66	C_5H_6	1,3-Cyclopentadiene	8.57	8.59	6.85E−03	1200	1600
68	C_5H_8	1,3-Pentadiene	8.59	8.59	5.53E−05	1200	1600
78	C_6H_6	Benzene	9.24	9.25	1.20E−02	1090	1600
	C_6H_6	Fulvene	8.36	8.38	7.13E−04	1200	1600
80	C_6H_8	1,3-Cyclohexadiene	8.25	8.19	2.05E−04	1200	1600
91	C_7H_7	Benzyl	7.24	None	1.10E−04	1200	1600
92	C_7H_8	Toluene	8.83	8.85	8.03E−04	1200	1600
102	C_8H_6	Phenylacetylene	8.82	8.92	3.81E−05	1200	1600
104	C_8H_8	Styrene	8.46	8.48	2.01E−04	1200	1600
106	C_8H_{10}	Ethylbenzene	7.90	7.80	1.67E−04	1200	1600
116	C_9H_8	Indene	8.14	8.15	7.51E−05	1370	1600
122	$C_{10}H_2$	1,3,5,7,9-Decapentayne	8.82	8.79	1.15E−05	1200	1600
136	$C_{10}H_{16}$	exo-TCD	9.35	9.22	2.97E−02		1090

[a] Reference to NIST ChemistryWebbook [48].
[b] The uncertainty for IEs is ±0.05 eV.
[c] X_M refers to the maximum mole fractions.
[d] T_{form} refers to the initial temperature for formation of species.
[e] T_M refers to the temperature corresponding to the maximum mole fraction.

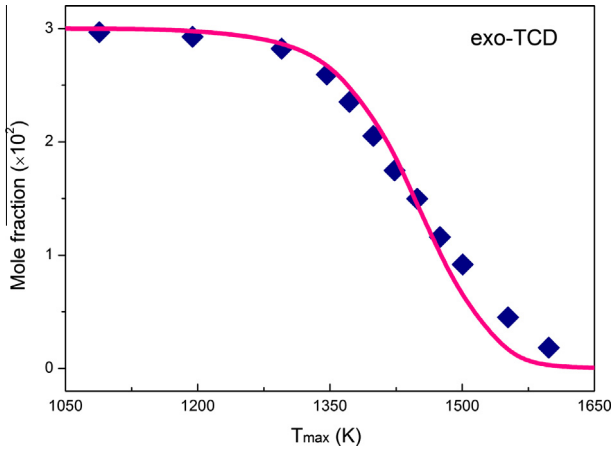

Fig. 4. Comparison between experimental and modeling mole fraction profiles of exo-TCD: exo-Tetrahydrodicyclopentadiene.

sites [7,13,57]. Apart from these two species, PC10, PC18 and PC12, derived from C1–C9 and C8–C9, are also the possible initial products for their formation channels via the transition states TS10, TS18 and TS12 with the lower activation energies of 81.90, 84.36 and 91.24 kcal mol^{-1}.

While the other species PC2–PC7, PC9, PC11 and PC13–PC17 formed via the corresponding transition states with higher energy barrier and give fewer yields, matching with their undetectable signal in experiment. PC2 and PC3 are formed from the C1–C2 bond scission via the transition state TS2 and TS3 with the energy barriers of 100.72 and 111.23 kcal mol^{-1}, which are higher than TS1, while PC4, PC5 and PC6 are derived from C2–C3 bond scission via the transition states TS4, TS5 and TS6 surmounting the energy barriers of 113.06, 113.17 and 110.27 kcal mol^{-1}. PC7 and PC17 are produced through C3–C4 bond scission via the transition states TS7 and TS17 with the energy barriers of 134.26 and 102.30 kcal mol^{-1}. PC9 and PC11 are derived from C1–C9 bond scission via the transition states TS9 and TS11 with the energy barriers of 100.57 and 124.55 kcal mol^{-1}, which are higher than TS18 or TS10. PC13 are formed from C8–C9 bond scission via the transition states TS13 with the energy barriers of 115.63 kcal mol^{-1} which is higher than TS12. Exo-TCD can also break C1–C6 bond and generate PC14, PC15 and PC16 via the transition states TS14, PC15 and PC16 with the energy barriers of 105.69, 132.64 and 99.03 kcal mol^{-1} respectively.

The calculation results imply that the decomposition pathways producing PC8, PC1, PC10, PC18 and PC12 may be the dominant channels in exo-TCD unimolecular decomposition reactions. In addition, the reaction pathways via diradicals are also considered in the process of exo-TCD decomposition, which are discussed in modeling Section 4.4. After the initial decomposition by C–C bond scission, the H abstraction reactions increase gradually, accelerating the decomposition of exo-TCD molecular simultaneously.

4.4. Modeling

The selected key reactions with each rate constant in this kinetic model of exo-TCD pyrolysis are listed in Table 1. The R1 and R2 (reactions 1 and 2) are diradical pathways derived from the pyrolysis mechanisms of Herbinet et al. [7,39]. The corresponding reverse rate constants for R1 and R2 are deduced from the values of rate constants at 1000 K. The temperature coefficient n is assumed to be zero and $k_{1000\ K}(R1_{-1}) = 1.3E+09\ s^{-1}$, $Ea(R1_{-1}) = 4.27$ kcal mol^{-1}; $k_{1000\ K}(R2_{-1}) = 3.8E+13\ s^{-1}$, $Ea(R2_{-1}) = 24$ kcal mol^{-1} [39,40]. Therefore, the approximate pre-exponential

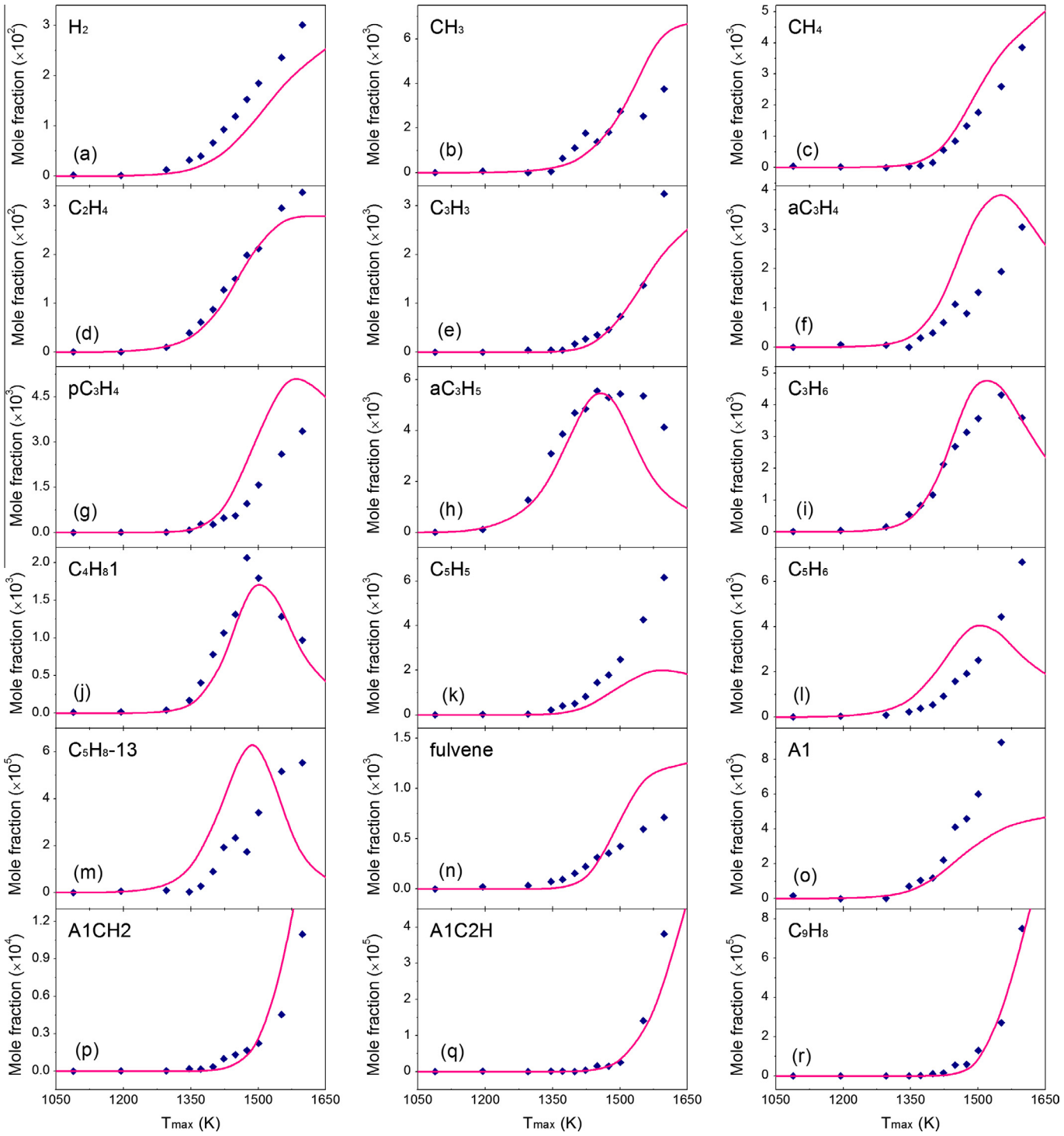

Fig. 5. Comparison between experimental and modeling mole fraction profiles of (a) H_2: Hydrogen, (b) CH_3: Methyl, (c) CH_4: Methane, (d) C_2H_4: Ethylene, (e) C_3H_3: Propargyl, (f) aC_3H_4: Allene, (g) pC_3H_4: Propyne, (h) aC_3H_5: Allyl, (i) C_3H_6: Propylene, (j) $C_4H_8$1: 1-Butene, (k) C_5H_5: Cyclopentadienyl, (l) C_5H_6: Cyclopentadiene, (m) C_5H_8-13: 1,3-Pentadiene, (n) Fulvene, (o) A1: Benzene, (p) A1CH2: Benzyl, (q) A1C2H: Phenylacetylene and (r) C_9H_8: Indene.

factor $A(R1_{-1}) = 1.1E+10$ and $A(R2_{-1}) = 6.7E+18$ deduced by the equation $k = AT^n exp(-E/RT)$. Besides, the computed rate constants for some possible unimolecular decomposition channels R5–R10 are fitted at the pressure 5 Torr and at the temperature range of 500–2000 K through the expression of modified Arrhenius equations. The reactions R5, R7–R10 correspond to the channels with relatively low barriers (TS1, TS10, TS12, TS18 and TS8) respectively. R6 is also added to this model for the comparison between producing CPCP-3 pathways from diradical reaction and unimolecular reaction.

The predicted mole fraction profiles of species were compared against experimental data as shown in Figs. 4 and 5. The products formed from the process of exo-TCD pyrolysis could provide some foundations for the initial dominant pathways. While, only limited number of species were identified and quantified in this experiment limited by the objective identification and analysis

conditions. The analysis for the predicted results compared with experimental profiles is discussed as follow.

4.4.1. Initial channels

The initial channels in this kinetic model include diradical initial reactions (R1 and R2) and unimolecular decomposition reactions (R5–R10). Figure S8 shows that the modeling results of exo-TCD decomposition against this experimental data applying Magoon model [15] (Mod.1) and current model (Mod.2 and Mod.3). The significant faster decomposition of reactant indicates that some initial mechanisms may not be suitable for this pyrolysis experiment at low pressure. Compared with the initial mechanisms from Herbinet et al. [7], the diradical mechanisms R1 and R2 in Magoon model [15] are lack of exact reverse rate constants. In this work, both forward and reverse rate constants of R1 and R2 are applied for modeling. As shown in Fig. S8, Mod.2 reflects that the direct modeling results of this model with no corrected rate constants of diradical mechanisms R1 and R2. Though exo-TCD decomposition from Mod.2 is slower than the results of Mod.1, it still seems to be faster and cannot predict the experimental data. The pressure (5 Torr, 3.0 vol.% exo-TCD in argon) of this work is much lower than that (760 Torr, 0.7–4% vol.% exo-TCD in helium) of the experiments conducted by Herbinet et al. [7]. The rate constants of initial diradical reactions may be slower due to the lower pressure. Mod.3 shows the improved modeling result of exo-TCD decomposition with the rate constants of R1 and R2 divided by five, which is consistent with the experimental data. This correction is applied in this modeling study.

The reaction pathway for exo-TCD pyrolysis at 1449 K is shown in Fig. 6. The exo-TCD decomposition mainly dominated by the diradical mechanism R1 based on ROP analysis. CPCP-3 is mainly formed by diradical reaction sequence exo-TCD → BR1 → CPCP-3 rather than the calculated unimolecular decomposition R6. The other reaction types including H abstraction and unimolecular decomposition contribute less to the consumption of exo-TCD as displayed in Fig. S9. Furthermore, the contribution of unimolecular decomposition reactions is not much sensitive to the increasing temperature compared with the diradical and H abstraction reactions. However, the contribution of diradical reactions consuming exo-TCD presents a trend of falling after first rise as the increasing temperature while that of H abstraction reactions shows an opposite trend at the same temperature range. The increasing of H radical and thus the activated chain reactions cause the increased contribution of H abstraction reactions for the consumption of exo-TCD after diradical initiation. The diradical reactions are competed and relatively inhibited by the increasing H abstraction reactions. Subsequently, some generated radicals continuously decompose to some small species or attack reactant molecular conversely for seizing H atom. These H abstraction reactions will flourish gradually to accelerate the radical chain reaction. Meanwhile, radical recombination pathway involved H radical also increases, which will capture some part of consumption flux of H radical and indirectly weaken some other channels consuming H radical. Therefore, when the temperature becomes much higher, the contribution of H abstraction reactions consuming exo-TCD drops slightly, which made the contribution of diradical reactions consuming exo-TCD increases correspondingly.

In addition, the sensitivity analysis of exo-TCD is described in Fig. 7, which indicates that diradical reactions (R1 and R23), H abstraction reactions (R11 and R13) show the promoting effects for the consumption of exo-TCD. R1 shows relative greater negative sensitivity. Meanwhile, R112 and R123 can supply H radical increasing H abstraction reactions to consume exo-TCD. In addition, R87 also shows the positive effect on exo-TCD consumption because it indirectly promotes CPCP-3 decomposition channel R23. While, R89 is a crucial indirect consumption channel of C_5H_7 competing with R112, which shows the adverse effect on the formation of H radical. H abstraction reactions R14 and R15 compete with the R11 and R13, which delay the exo-TCD consumption.

Exo-TCDJ3 is the largest amount of C10H15 species formed from H abstraction reactions base on ROP analysis. Figure 8 shows the sensitivity analysis of exo-TCDJ3. The major formation channel of exo-TCDJ3 (R13) and some reactions supplying H radicals (R112 and R123) show the positive effects on the formation of

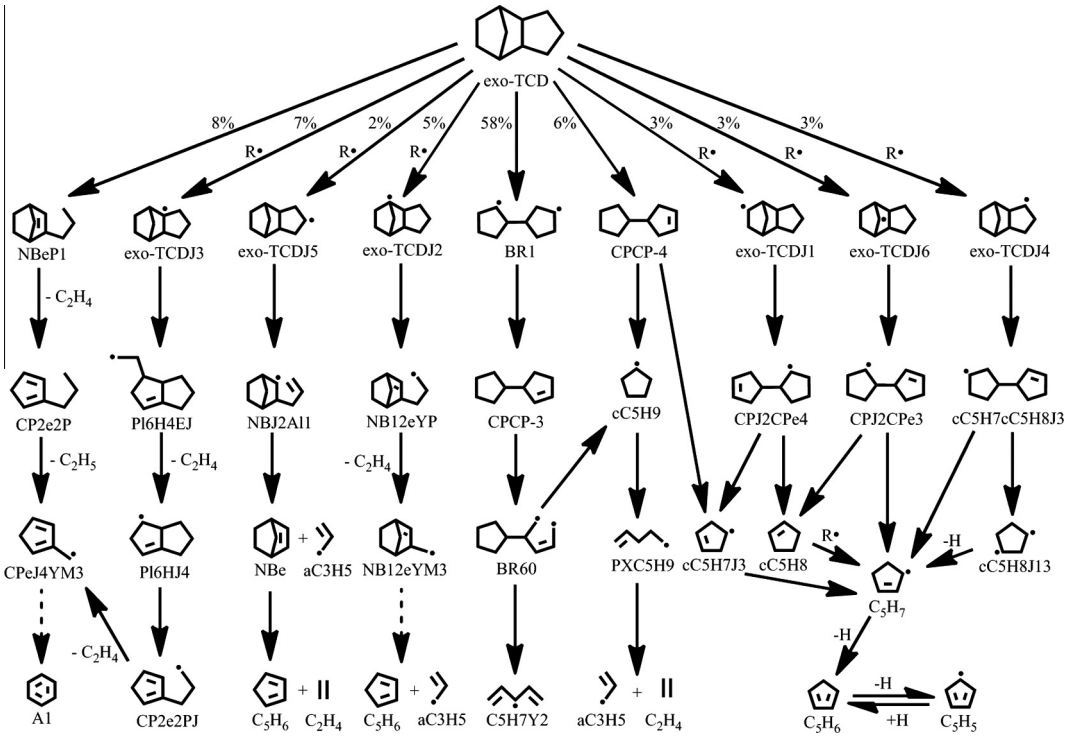

Fig. 6. The reaction pathway for exo-TCD pyrolysis at 1449 K. The conversion of exo-TCD is 54% approximately. The numbers indicate the conversion percentage.

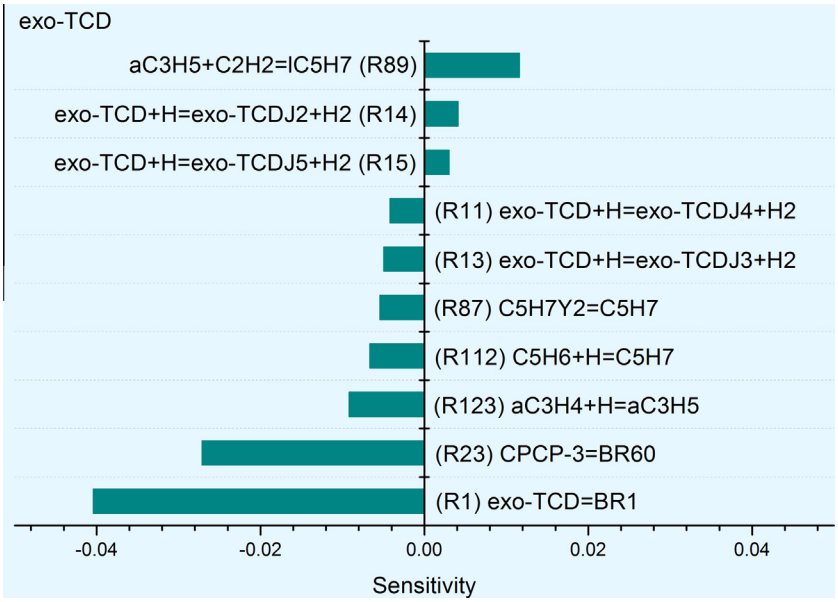

Fig. 7. Sensitivity analysis of exo-TCD in exo-TCD pyrolysis at 1449 K. The conversion of exo-TCD is 54% approximately. Reactions with absolute sensitivity coefficients higher than 0.002 are considered.

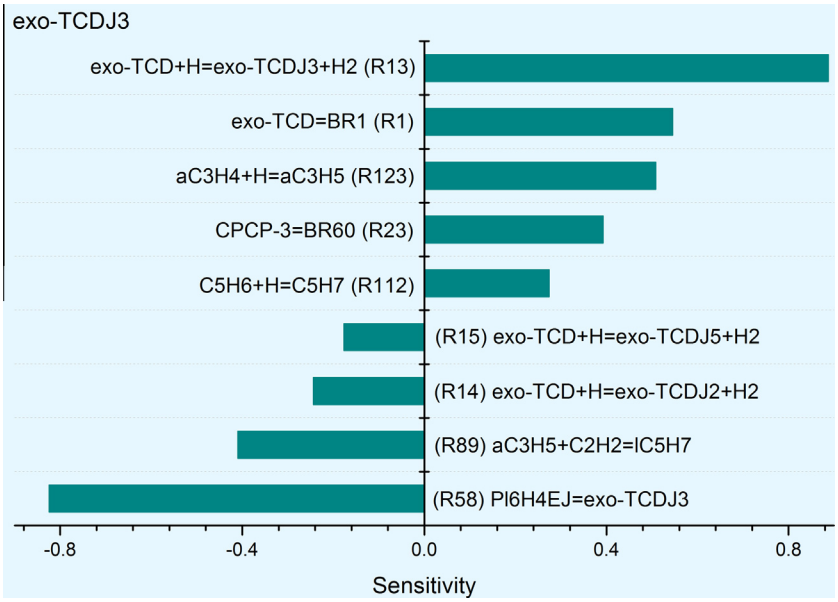

Fig. 8. Sensitivity analysis of exo-TCDJ3 in exo-TCD pyrolysis at 1449 K. The conversion of exo-TCD is 54% approximately. Reactions with absolute sensitivity coefficients higher than 0.02 are considered.

exo-TCDJ3. R1 and R23 as the indirect reactions producing H radicals through R112 also promote exo-TCDJ3 formation. While, the direct consumption reaction R58 and H abstraction reactions R14 and R15 competing with R13 for consuming H radicals show the adverse effect on the formation of exo-TCDJ3. R89 can consume C5H7 indirectly through R87 and R88, which decreases R112 and inhibits exo-TCDJ3 formation. Other C10H15 species have the relatively similar formation and consumption feature related to exo-TCD and H radical.

4.4.2. C0–C5 species

The primary initial decomposition channels of exo-TCD are diradical reactions (R1 and R3), H abstraction reactions (R11–R16) and unimolecualr reactions (R5 and R7). The major exo-TCD consumption route is exo-TCD → BR1 → CPCP-3.

In this experiment, the main C0–C2 species of hydrogen (H_2), methyl (CH_3), methane (CH_4), ethylene (C_2H_4) and acetylene (C_2H_2). Only hydrogen is under-predicted which may be caused by the inexact rate constants of some H abstraction reactions. C_2H_4 and C_2H_2 are mainly from the channels R138 and R89 respectively. While, the simulated mole fraction value of acetylene is much higher than the experimental data. That may be lack of some consumption pathways of acetylene in this model.

The predicted formation of H radical is mainly derived from the radical dehydrogenation channels (R83 SAXcC6H7 = A1 + H, R142 $H + C_2H_4(+M) = C_2H_5(+M)$, R123 $aC_3H_4 + H = aC_3H_5$, R105 $C_5H_7 + H = cC_5H_8J13$ and R112 $C_5H_6 + H = C_5H_7$), while its consumption is through the channels (R13 exo-TCD + H = exo-TCDJ3 + H2, R106 $H + cC_5H_8 = H_2 + C_5H_7$, R122 $aC_3H_5 + H(+M) = C_3H_6(+M)$, R135 $C_2H_3 + CH_3 = aC_3H_5 + H$, R92 $C_5H_6 + H = C_5H_5 + H2$

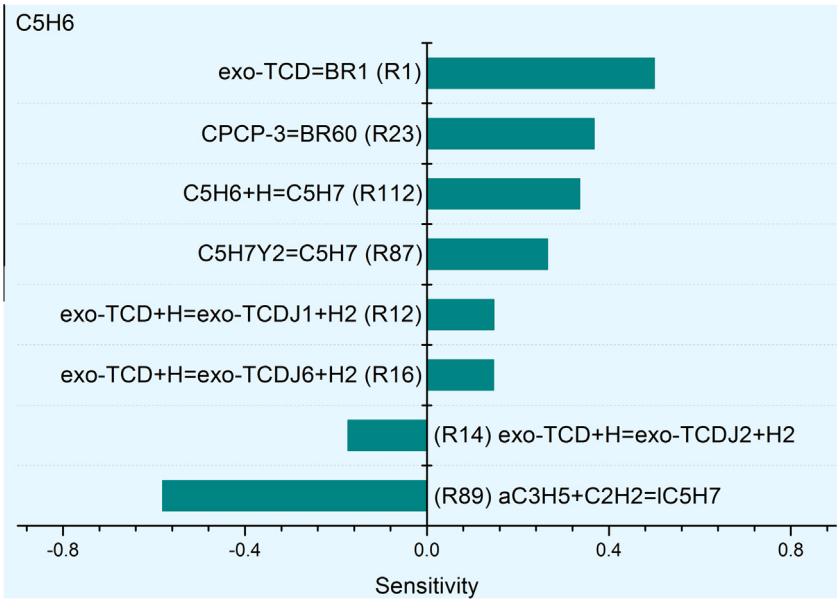

Fig. 9. Sensitivity analysis of cyclopentadiene in exo-TCD pyrolysis at 1449 K. The conversion of exo-TCD is 54% approximately. Reactions with absolute sensitivity coefficients higher than 0.02 are considered.

and R94 $C_5H_5 + H = C_5H_6$). Larger amount of H radicals can speeds up exo-TCD decomposition.

The major C3–C4 species contain allyl (aC_3H_5), allene (aC_3H_4), propyne (pC_3H_4), propargyl or CH2CCH (C_3H_3), propane (C_3H_6), 1-buten-3-yne(C_4H_4) and 1-butene(C_4H_81). Fig. 5(e)–(j) shows that the predicted mole fraction profiles of C_3H_3, aC_3H_5, C_3H_6, C_4H_81 are consistent with the experimental data apart from aC_3H_4, pC_3H_4 and C_4H_4. The over-prediction of them may be caused by the lack of some consumption pathways. ROP analysis shows that the decomposition of lC_5H_7 and PXC_5H_9 (R89 and R138) contribute over 90% to the formation of aC_3H_5. aC_3H_5 can generate C_3H_6, C_4H_81, aC_3H_4 and pC_3H_4 by R122, R119, R123 and R121 respectively. C_4H_81 (1-butene) is mainly formed by the recombination of aC_3H_5 and CH_3 (R119). C_4H_4 is mainly produced by the recombination and dehydrogenation of C_2H_3 and C_2H_2. Almost all of aC_3H_4 is derived from the dehydrogenation of aC_3H_5 (R123, R128 and R129). aC_3H_4 mainly generates pC_3H_4 by hydroisomerization (R136) and C_3H_3 by H abstraction (R126). Apart from the consumption of aC3H4 (R125 and R136), pC_3H_4 is generated by R121 and R124 below 1346 K. pC_3H_4 will produce C_3H_3 by H abstraction (R130) or decompose to CH_3 and C_2H_2 by hydrogenolysis (R132). C_3H_3 mainly formed by R126 and R130 can generate some part of fulvene (R133) and a little benzene (R80) at high temperature.

The identified C5 species are 1,3-pentadiene (C_5H_8-13), cyclopentadiene (C_5H_6) and cyclopentadienyl (C_5H_5). C_5H_6 and C_5H_5 account for the majority of C5 species, which is consistent with the results of Herbinet et al. Cyclopentyl (cC_5H_9) is generated by the decomposition of CPCP-3 and CPCP-4 (R23, R24 and R25) and then quickly produces 1-penten-5-yl (PXC_5H_9) by ring-open (R111) (see Fig. 6). Cyclopentene (cC_5H_8) is mainly formed from the reaction sequences of exo-TCDJ1 → CPJ2CPe4 → cC_5H_8 and exo-TCDJ6 → CPJ2CPe3 → cC_5H_8 from exo-TCDJ1 and exo-TCDJ6. cC_5H_7J3 can be produced by the decomposition of CPCP-4 (R25) and CPJ2CPe4 (R53). ROP analysis shows that almost all of cC_5H_7J3 can isomerize to cyclopentenyl (C_5H_7) (R103 and R104), lots of cC_5H_8 produces C_5H_7 by R106 and small part of cC_5H_8 produces C_5H_8-13 by R108 and R109. C_5H_7 is a primary C5 intermediate generated by cC_5H_7J3 isomerization (R103, R104), the dehydrogenation of cC_5H_8J13 (R105), H abstraction of cC_5H_8 (R106) and the decomposition of CPJ2CPe3 and cC5H7cC5H8J3 (R71 and R56).

C_5H_8-13 is derived from the isomerizaion of cC_5H_8. As shown in Fig. 5(m), the maximum mole fraction of C_5H_8-13 is consistent with the experimental data though its formation temperature is shifted toward lower temperature. ROP analysis shows that C_5H_8-13 formation is mainly derived from the dehydrogenation and isomerization of 1-penten-5-yl (PXC5H9) (R110) at 1087 K and the ring-open and isomerization of cC_5H_8 (R108 and R109) at the temperature range of 1346–1551 K. PXC_5H_9 is the main ring-open (R111) product of cC_5H_9.

ROP analysis indicates that the formation pathway of C_5H_6 mainly includes the reactions R112, R70 and R94. Figure 5(k)–(l) shows that the predicted mole fraction profiles of C_5H_6 is higher than experimental data before 1500 K while that of C_5H_5 is lower than experimental data. And the predicted mole fraction profiles of C_5H_6 and C_5H_5 are both insufficient above 1500 K. That may be caused by the inexact rate constants of the reverse reactions of R112 and R70 producing C_5H_6. The dehydrogenation of C_5H_7 (R112) contribute the majority for C_5H_6 formation, only a little C_5H_6 is derived from the addition of C_5H_5 and H radical (R94) and retra-Diels–Alder reaction of norbornene (R70). Meanwhile, R112 has a positive effect on C_5H_6 production, as seen the sensitivity analysis of C_5H_6 in Fig. 9. Besides, the diradical reactions (R1 and R23) and isomerization R87 can indirectly promote the formation pathway R112 of C_5H_6 through the reaction sequence (R1 → R3 → R23 → R24 → R87). H abstraction reactions R12 and R16 are both key formation source of C_5H_7 promoting C_5H_6 formation while R14 is not a formation source of C_5H_7 and competes with R12 and R16 so that it has the decreased effect on C_5H_6 formation. R89 also inhibits C_5H_6 formation because it can consume C_5H_7 indirectly by the reaction sequence (R87 → R88 → R89). Most of C_5H_6 produces C_5H_5 by H abstraction reaction (R92), which is also the main formation source of C_5H_5. The major consumption of C_5H_5 is the addition with H radical to produce C_5H_6 (R94) above 1346 K. Most of C_5H_5 isomerizes to the linear C_5H_5 species (R97) producing C_2H_3, C_3H_3, C_5H_4, H_2 and CH_4 by R100, R101 and R102. The rest of C_5H_5 will produces benzyl via the addition reaction with C_2H_2 (R99) or produce cC_5H_4 through H abstraction reaction (R98) at

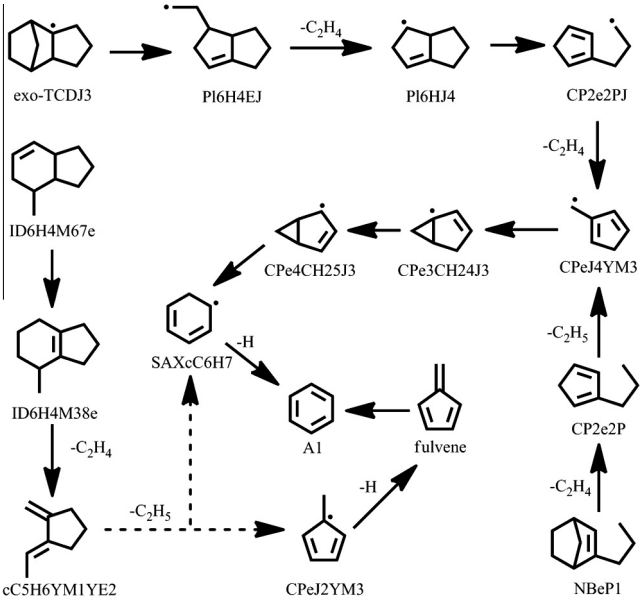

Fig. 10. The important formation pathways of benzene predicted by this kinetic model at 1449 K.

the temperature below 1346 K. The primary consumption channels of C_5H_6 (R92) and C_5H_5 (R94) not only compete with each other but also affected by the formation and consumption channels of H radical simultaneously, which is the main reason for the flux drop of C_5H_6 and C_5H_5 consumption with H radical (R92 and R94) at the temperature range of 1449–1551 K.

4.4.3. C6 species

The primary C6 species in this experiment are benzene and fulvene. The main formation mechanisms of benzene are selected and applied in this model including SAXcC6H7 = A1 + H (R83), fulvene + H = A1 + H (R84) and $C_3H_3 + C_3H_3$ = A1 (R80). Benzene formation pathways in exo-TCD pyrolysis are derived from the initial C–C bond scission and C–H bond scission. One pathway is the isomerization and dehydrogenation of methylene-cyclic C5 species originated from exo-TCDJ3 decomposition, which had been reported by Herbinet et al. [7]. While another is derived from the dehydrogenation and ethylene elimination of a cyclic C8 intermediate originated from the C2–C3 scission of exo-TCD molecular proposed by Bozzelli et al. [57]. The two mechanisms are similarly applied in this model. The formation temperature of benzene is 1090 K and the accumulated mole fraction values of benzene as the increasing temperature seems a little higher than any other experimental data published at different reaction conditions. Based on the ROP analysis, the pathway derived from fulvene (R84) only contributes a little part of benzene formation at high temperature. Benzene may be formed by some species originated from the initial products for its formation at low temperature. A probable pathway may be originated from NBeP1, an intermediate generated by the initial channel (R7) with a lower potential energy (see Fig. S6). Furthermore, Fig. 10 shows that NBeP1 quickly decomposes to an ethylene and 2-propylcyclopentadiene (CP2e2P) through a retro-Diels–Alder reaction (R26). A methylene-cyclicC5 species (CPeJ4YM3) can be generated from CP2e2P with ethyl elimination (R27). CPeJ4YM3 subsequently experiences an isomerization sequence (R28 → R29 → R30) to generate cyclohexadienyl (SAXcC6H7) which could produce benzene easily through dehydrogenation (R83). ROP analysis shows that this pathway is a key formation route of benzene as the increasing temperature. However, some other pathways of benzene formation may also exist. Figure 10 displays that some other initial products including exo-TCDJ3 and ID6H4M67e are the possible source species of benzene formation. The beta-scission of exo-TCDJ3 generates Pl6H4EJ which could produce Pl6HJ4 with ethylene elimination. Similarly, CP2e2PJ formed by the beta-scission of Pl6HJ4 can generate ethylene and CPeJ4YM3 which is an intermediate of benzene formation. ID6H4M67e can suffer an isomerization process to produce ID6H4M38e which will decompose to cC5H6YM1YE2 and ethylene by a retro-Diels–Alder reaction. cC5H6YM1YE2 can suffer the intramolecular H-transfer to form some ethyl-methyl-cyclicC5 or ethyl-methylene-cyclicC5 species which could produce CPeJ2YM3 or SAXcC6H7 by the process of isomerization and ethyl elimination. Fulvene and benzene can be formed by dehydrogenation of CPeJ2YM3 and SAXcC6H7 respectively and they can isomerize to each other. In summary, methyl-cyclicC5 and methylene-cyclicC5 species may be the important class of intermediates leading to benzene formation by isomerization and dehydrogenation. The ROP analysis also shows that only a little benzene is generated from fulvene and C_3H_3 (R84 and R80). The H-assisted isomerization of fulvene (R84) is the main consumption channel of fulvene, which increases as the accumulated fulvene. The increasing proportion of the recombination of C_3H_3 (R80) is mainly caused by the intensifying chain termination as the increasing temperature. As shown in Fig. 5(n)–(o), the simulated concentration of fulvene is somewhat over-predicted above 1450 K while that of benzene is under-predicted above 1400 K. That may be due to the lack of some benzene formation mechanisms in the current model and some fulvene or its source species should have convert to benzene.

4.4.4. C7–C9 aromatic species

The predicted mole profiles of the aromatic species phenyl ($A1CH_2$), phenylacetylene ($A1C_2H$) and indene (C_9H_8) are consistent with the experimental data within the accepted error range (see Fig. 5(p)–(r)). Phenyl (A1–) is an intermediate for the formation of aromatic hydrocarbon in exo-TCD pyrolysis. ROP analysis shows that the formation of indene is derived from the recombination and dehydrogenation of A1– and aC_3H_4/$A1CH_2$ and C_2H_2/A1 and C_3H_3 (R147/R150/R79), the recombination of A1– and C_3H_3 (R149) or dehydrogenation (R148). C_9H_8 can produce C_9H_7 through H abstraction (R144 and R146) or dehydrogenation (R145). $A1CH_2$ is mainly generated by the reverse channel $A1CH_2 + H = A1– + CH_3$. $A1C_2H$ is mainly generated by $A1– + C_2H_2 = A1C_2H + H$ and $A1 + C_2H = A1C_2H + H$.

5. Conclusion

An experiment of exo-TCD pyrolysis at low pressure was studied employing SVUV-PIMS over the temperature range of 900–1600 K at low pressure. The majority species from pyrolysis process were detected and indentified including radicals and isomers. The mole fractions of them are determined. Some unimolecular decomposition channels of exo-TCD were studied by quantum chemical calculation and the corresponding rate constants were computed based on the RRKM/master equation method. Furthermore, a detailed kinetic model for exo-TCD pyrolysis was developed containing 316 species and 807 reactions to simulate exo-TCD pyrolysis of this work. The relative consistency of predicted and experimental mole fraction profiles reflects the applicability of this model. The main decomposition pathway of exo-TCD pyrolysis is described by ROP and sensitivity analysis. The comparison of experimental and simulated data indicates that the reactions exo-TCD = BR1 and BR1 = CPCP-3 are dominant pathway of exo-TCD decomposition at low pressure. The decomposition of CPCP-3 mainly produces C_5H_6, aC_3H_5 and C_2H_4. The calculated unimolecular decomposition pathways contribute little to exo-TCD decomposition. The dominant formation pathway of

benzene may be the isomerization and dehydrogenation of methyl-cyclicC5 and methylene-cyclicC5 species in exo-TCD pyrolysis.

Acknowledgments

The authors gratefully acknowledge National Synchrotron Radiation Laboratory of China for the funding and technical supports and Prof. F. Qi, Dr. Lidong Zhang and Dr. Feng Zhang for their help in this work. The authors are also grateful to Wenhao Yuan, Lili Ye, Jiuzhong Yang and Xiaoyuan Zhang for their technical assistance. This research is financially supported by National Natural Science Fund of China (U1232134) and Program for New Century Excellent Talents (NCET-13-0408).

Appendix A. Supplementary material

Supplementary data associated with this article can be found, in the online version, at http://dx.doi.org/10.1016/j.combustflame.2015.01.015.

References

[1] D.F. Davidson, D.C. Horning, M.A. Oehlschlaeger, R.K. Hanson, The decomposition products of JP-10, in: 37th AIAA JPC, Salt Lake City, July 2001.
[2] T. Edwards, J. Propul. Power 19 (2003) 1089–1107.
[3] H. Huang, L.J. Spadaccini, D.R. Sobel, J. Eng. Gas Turbines Power-Trans. Asme 126 (2004) 284–293.
[4] M. Cooper, J.E. Shepherd, GALCIT Report FM 2002.002, California Institute of Technology, Pasadena, CA, 2002.
[5] D.F. Davidson, D.C. Horning, J.T. Herbon, R.K. Hanson, Proc. Combust. Inst. 28 (2000) 1687–1692.
[6] S.C. Li, B. Varatharajan, F.A. Williams, AIAA J. 39 (2001) 2351–2356.
[7] O. Herbinet, B. Sirjean, R. Bounaceur, R. Fournet, F. Battin-Leclerc, G. Scacchi, P.M. Marquaire, J. Phys. Chem. A 110 (2006) 11298–11314.
[8] P.N. Rao, D. Kunzru, J. Anal. Appl. Pyrolysis 76 (2006) 154–160.
[9] S. Nakra, R.J. Green, S.L. Anderson, Combust. Flame 144 (2006) 662–674.
[10] T.J. Bruno, M.L. Huber, A. Laesecke, E.W. Lemmon, R.A. Perkins, NIST-IR 6640, National Institute of Standards and Technology (U.S.A.), 2006.
[11] K. Chenoweth, A.C.T. van Duin, S. Dasgupta, W.A. Goddard III, J. Phys. Chem. A 113 (2009) 1740–1746.
[12] C.Q. Jiao, C.A. DeJoseph Jr., A. Garscadden, Int. J. Mass Spectrom. 266 (2007) 92–96.
[13] S.H. Park, C.H. Kwon, J. Kim, B.H. Chun, J.W. Kang, J.S. Han, B.H. Jeong, S.H. Kim, Ind. Eng. Chem. Res. 49 (2010) 8319–8324.
[14] N.M. Vandewiele, G.R. Magoon, K.M. Van Geem, M.-F. Reyniers, W.H. Green, G.B. Marin, Energy Fuels 28 (2014) 4976–4985.
[15] G.R. Magoon, J. Aguilera-Iparraguirre, W.H. Green, J.J. Lutz, P. Piecuch, H.W. Wong, O.O. Oluwole, Int. J. Chem. Kinet. 44 (2012) 179–193.
[16] G.R. Magoon, W.H. Green, O.O. Oluwole, H.W. Wong, S.E. Albo, D.K. Lewis, Updating our understanding of JP-10 decomposition chemistry: a detailed JP-10 combustion mechanism constructed using RMG – an automatic reaction mechanism generator, in: 46th AIAA/ASME/SAE/ASEE Joint Propulsion Conference and Exhibit, Nashville, TN, July 25–28, 2010.
[17] Y. Xing, W. Fang, W. Xie, Y. Guo, R. Lin, Ind. Eng. Chem. Res. 47 (2008) 10034–10040.
[18] T.C. Zhang, J. Wang, T. Yuan, X. Hong, L.D. Zhang, F. Qi, J. Phys. Chem. A 112 (2008) 10487–10494.
[19] T.C. Zhang, L.D. Zhang, J. Wang, T. Yuan, X. Hong, F. Qi, J. Phys. Chem. A 112 (2008) 10495–10501.
[20] T.C. Zhang, L.D. Zhang, X. Hong, K.W. Zhang, F. Qi, C.K. Law, T.H. Ye, P.H. Zhao, Y.L. Chen, Combust. Flame 156 (2009) 2071–2083.
[21] Y.Y. Li, Z.Y. Tian, L.D. Zhang, T. Yuan, K.W. Zhang, B. Yang, F. Qi, Proc. Combust. Inst. 32 (2009) 647–655.
[22] Y.Y. Li, L.D. Zhang, Z.Y. Tian, T. Yuan, J. Wang, B. Yang, F. Qi, Energy Fuels 23 (2009) 1473–1485.
[23] Y.Y. Li, L.D. Zhang, T. Yuan, K.W. Zhang, J.Z. Yang, B. Yang, F. Qi, C.K. Law, Combust. Flame 157 (2010) 143–154.
[24] J.J. Zou, Y. Xu, X.W. Zhang, L. Wang, Appl. Catal., A 421–422 (2012) 79–85.
[25] L. Wang, J.J. Zou, X.W. Zhang, Fuel 91 (2012) 164–169.
[26] G.Z. Liu, Z.T. Mi, L. Wang, X.W. Zhang, S.T. Zhang, Ind. Eng. Chem. Res. 45 (2006) 8807–8814.
[27] F. Qi, Proc. Combust. Inst. 34 (2013) 33–63.
[28] J.H. Cai, L.D. Zhang, F. Zhang, Z.D. Wang, Z.J. Cheng, W.H. Yuan, F. Qi, Energy Fuels 26 (2012) 5550–5568.
[29] Y.J. Zhang, J.H. Cai, L. Zhao, J.Z. Yang, H.F. Jin, Z.J. Cheng, Y.Y. Li, L.D. Zhang, F. Qi, Combust. Flame 159 (2012) 905–917.
[30] M. Kamphus, N.N. Liu, B. Atakan, F. Qi, A. McIlroy, Proc. Combust. Inst. 29 (2002) 2627–2633.
[31] J.A. Montgomery Jr., M.J. Frisch, J.W. Ochterski, G.A. Petersson, J. Chem. Phys. 110 (1999) 2822–2827.
[32] J.A. Montgomery Jr., M.J. Frisch, J.W. Ochterski, G.A. Petersson, J. Chem. Phys. 112 (2000) 6532–6542.
[33] J.B. Foresman, A. Frisch, Exploring Chemistry with Electronic Structure Methods, second ed., Gaussian, Pittsburgh, PA, 1996.
[34] M.J. Frisch, G.W. Trucks, H.B. Schlegel, G.E. Scuseria, M.A. Robb, J.R. Cheeseman, G. Scalmani, V. Barone, B. Mennucci, G.A. Petersson, H. Nakatsuji, M. Caricato, X. Li, H.P. Hratchian, A.F. Izmaylov, J. Bloino, G. Zheng, J.L. Sonnenberg, M. Hada, M. Ehara, K. Toyota, R. Fukuda, J. Hasegawa, M. Ishida, T. Nakajima, Y. Honda, O. Kitao, H. Nakai, T. Vreven, J.A. Montgomery Jr., J.E. Peralta, F. Ogliaro, M. Bearpark, J.J. Heyd, E. Brothers, K.N. Kudin, V.N. Staroverov, T. Keith, R. Kobayashi, J. Normand, K. Raghavachari, A. Rendell, J.C. Burant, S.S. Iyengar, J. Tomasi, M. Cossi, N. Rega, J.M. Millam, M. Klene, J.B.C.J.E. Knox, V. Bakken, C. Adamo, J. Jaramillo, R. Gomperts, R.E. Stratmann, O. Yazyev, A.J. Austin, R. Cammi, C. Pomelli, J.W. Ochterski, R.L. Martin, K. Morokuma, V.G. Zakrzewski, P.S.G.A. Voth, J.J. Dannenberg, S. Dapprich, A.D. Daniels, O. Farkas, J.B. Foresman, J.V. Ortiz, J. Cioslowski, D.J. Fox, Gaussian 09, Revision B.02 Inc., Wallingford CT, 2010.
[35] V. Mokrushin, V. Bedanov, W. Tsang, M. Zachariah, V. Knyazev, ChemRate, version 1.5.2 National Institute of Standards and Testing: Gaithersburg, MD, 2006.
[36] L.S. Tee, S. Gotoh, W.E. Stewart, Ind. Eng. Chem. Fundam. 5 (1966) 356–363.
[37] K.S. Pitzer, D.Z. Lippmann, R. Curl Jr., C.M. Huggins, D.E. Petersen, J. Am. Chem. Soc. 77 (1955) 3433–3440.
[38] G. da Silva, J.A. Cole, J.W. Bozzelli, J. Phys. Chem. A 113 (2009) 6111–6120.
[39] O. Herbinet, Experimental and Modeling Studies of the Thermal Decomposition of l'exo-tricyclo[5.2.1.0(2.6)]decane, Institut National Polytechnique de Lorraine-INPL, 2006.
[40] H. O'Neal, S.W. Benson, Int. J. Chem. Kinet. 2 (1970) 423–456.
[41] L.D. Zhang, J.H. Cai, T.C. Zhang, F. Qi, Combust. Flame 157 (2010) 1686–1697.
[42] J. Song, S. Raman, J. Yu, C.D. Wijaya, G. Stephanopoulos, W.H. Green, RMG: the next generation of automatic chemical reaction mechanism generator, in: proceedings AIChE Annual Meeting, San Francisco, CA, USA, 2003.
[43] Z.D. Wang, Z.J. Cheng, W.H. Yuan, J.H. Cai, L.D. Zhang, F. Zhang, F. Qi, J. Wang, Combust. Flame 159 (2012) 2243–2253.
[44] G.P. Smith, D.M. Golden, F. Frenklach, N.W. Moriarty, B. Eiteneer, M. Goldenberg, C.T. Bowman, R.K. Hanson, S. Song, W.C.J. Gardiner, V.V. Lissianski, Z. Qin, GRI-Mech 3.0, 1999, <http://www.me.berkeley.edu/grimech>.
[45] H. Wang, E. Dames, B. Sirjean, D.A. Sheen, R. Tangko, A. Violi, J.Y.W. Lai, F.N. Egolfopoulos, D.F. Davidson, R.K. Hanson, C.T. Bowman, C.K. Law, W. Tsang, N.P. Cernansky, D.L. Miller, R.P. Lindstedt, A High-temperature Chemical Kinetic Model of n-alkane (up to n-dodecane), Cyclohexane, and Methyl-,ethyl-, n-propyl and n-butyl-cyclohexane Oxidation at High Temperatures, JetSurF Version 2.0, September 19, 2010. <http://melchior.usc.edu/JetSurF/JetSurF2.0>.
[46] CHEMKIN-PRO 15092, Reaction Design, San Diego, 2009.
[47] Y.Y. Li, F. Qi, Acc. Chem. Res. 43 (2009) 68–78.
[48] P.J. Linstrom, W.G. Mallard, NIST Chemistry Webbook, National Institute of Standard and Technology, Number 69, Gaithersburg, MD, 2005. Available from: <http://webbook.nist.gov/>.
[49] B. Yang, J. Wang, T.A. Cool, N. Hansen, S. Skeen, D.L. Osborn, Int. J. Mass Spectrom. 309 (2012) 118–128.
[50] T. Adam, R. Zimmermann, Anal. Bioanal. Chem. 389 (2007) 1941–1951.
[51] S. Soorkia, A.J. Trevitt, T.M. Selby, D.L. Osborn, C.A. Taatjes, K.R. Wilson, S.R. Leone, J. Phys. Chem. A 114 (2010) 3340–3354.
[52] T. Bally, D. Hasselmann, K. Loosen, Helv. Chim. Acta 68 (1985) 345–354.
[53] Z.Y. Zhou, M.F. Xie, Z.D. Wang, F. Qi, Rapid Commun. Mass Spectrom. 23 (2009) 3994–4002.
[54] N. Hansen, S.J. Klippenstein, J.A. Miller, J. Wang, T.A. Cool, M.E. Law, P.R. Westmoreland, T. Kasper, K. Kohse-Höinghaus, J. Phys. Chem. A 110 (2006) 4376–4388.
[55] C.A. Taatjes, D.L. Osborn, T.M. Selby, G. Meloni, A.J. Trevitt, E. Epifanovsky, A.I. Krylov, B. Sirjean, E. Dames, H. Wang, J. Phys. Chem. A 114 (2010) 3355–3370.
[56] J.M. Hudzik, R. Asatryan, J.W. Bozzelli, J. Phys. Chem. A 114 (2010) 9545–9553.
[57] J.W. Bozzelli, A. Castillo, J. Hudzik, Exo-tricyclo[5.2.1.$0^{2,6}$]decane (TCD or JP-10) decomposition: thermochemistry and kinetics of ring opening and formed intermediates, in: the 244th ACS National Meeting, Philadelphia, PA, 2012.
[58] S.J. Klippenstein, L.B. Harding, Y. Georgievskii, Proc. Combust. Inst. 31 (2007) 221–229.
[59] H. Wang, X. You, A.V. Joshi, S.G. Davis, A. Laskin, F. Egolfopoulos, C.K. Law, USC Mech Version II, High-Temperature Combustion Reaction Model of H2/CO/C1-C4 Compounds, 2007, <http://ignis.usc.edu/USC_Mech_II.htm.
[60] C. Chanmugathas, J. Heicklen, Int. J. Chem. Kinet. 18 (1986) 701–718.
[61] N. Hansen, J.A. Miller, T. Kasper, K. Kohse-Hoinghaus, P.R. Westmoreland, J. Wang, T.A. Cool, Proc. Combust. Inst. 32 (2009) 623–630.
[62] W.J. Li, M.E. Law, P.R. Westmoreland, T. Kasper, N. Hansen, K. Kohse-Hoinghaus, Combust. Flame 158 (2011) 2077–2089.
[63] I. Ziegler, R. Fournet, P.-M. Marquaire, J. Anal. Appl. Pyrolysis 73 (2005) 212–230.
[64] K.D. King, Int. J. Chem. Kinet. 10 (1978) 117–123.
[65] G.B. Bacskay, J.C. Mackie, Phys. Chem. Chem. Phys. 3 (2001) 2467–2473.
[66] J. Kiefer, K. Gupte, L. Harding, S. Klippenstein, J. Phys. Chem. A 113 (2009) 13570–13583.
[67] G. Blanquart, P. Pepiot-Desjardins, H. Pitsch, Combust. Flame 156 (2009) 588–607.
[68] E. Pousse, P.A. Glaude, R. Fournet, F. Battin-Leclerc, Combust. Flame 156 (2009) 954–974.